Adsorption characteristics and mechanisms of water-soluble polymers (PVP and PEG) on kaolin and montmorillonite minerals

Xintu Wang [a,b,1], Yanghui Xu [b,c,1], Qin Ou [b,c], Wenwen Chen [a], Walter van der Meer [d,e], Gang Liu [b,c,f,*]

[a] The Guangxi Key Laboratory of Theory and Technology for Environmental Pollution Control, Guilin University of Technology, Guilin 541006, China
[b] Key Laboratory of Drinking Water Science and Technology, Research Centre for Eco-Environmental Sciences, Chinese Academy of Sciences, Beijing 100085, China
[c] Section of Sanitary Engineering, Department of Water Management, Faculty of Civil Engineering and Geosciences, Delft University of Technology, Stevinweg 1, 2628 CN Delft, the Netherlands
[d] Science and Technology Faculty, Twente University, Enschede 7500AE, the Netherlands
[e] Oasen Drinkwater, Gouda 2800 AC, the Netherlands
[f] University of Chinese Academy of Sciences, Beijing, China

HIGHLIGHTS

- WSPs (PEG and PVP) adsorption on kaolin and montmorillonite minerals was assessed.
- Hydrogen bond and van der Waals force dominated the adsorption of WSPs.
- The adsorption of WSPs depended on their molecular weight and mineral pore size.
- PEG of all molecular weights (<10 kDa) could penetrate the internal spaces of both minerals.
- High molecular weight PVP was restricted to the external surface of montmorillonite.

GRAPHICAL ABSTRACT
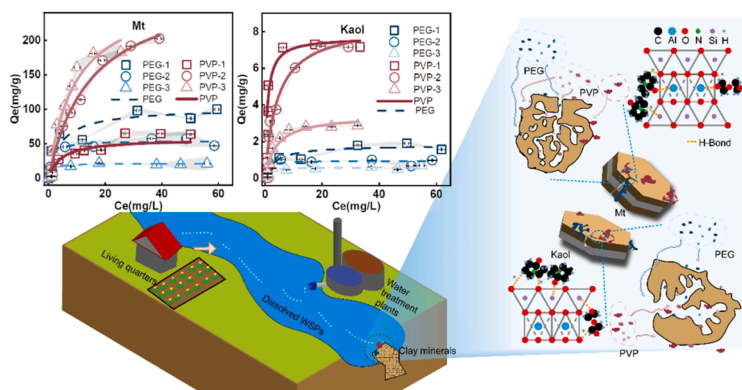
ARTICLE INFO

ABSTRACT

The excessive use and accumulation of water-soluble polymers (WSPs, known as "liquid plastics") in the environment can pose potential risks to both ecosystems and human health, but the environmental fate of WSPs remains unclear. Here, the adsorption behavior of WSPs with different molecular weight on kaolinite (Kaol) and montmorillonite (Mt) were examined. The results showed that the adsorption of PEG and PVP on minerals were controlled by hydrogen bond and van der Waals force. The Fourier transform infrared (FTIR) spectra and two-dimensional correlation spectroscopy (2D-COS) analysis revealed that there were interactions between the Al-O and Si-O groups of the minerals and the polar O- or N-containing functional groups as well as the alkyl groups of PEG and PVP. The adsorption characteristics of WSPs were closely related to their molecular weight

---

* Correspondence to: Research Center for Eco-Environmental Sciences, Chinese Academy of Sciences, Sanitary Engineering, CiTG, Delft University of Technology, China.
  E-mail addresses: gliu@rcees.ac.cn, g.liu-1@tudelft.nl (G. Liu).
  [1] Xintu Wang and Yanghui Xu contributed equally to this manuscript.

and the pore size of minerals. Due to the relatively large mesopore size of Kaol, both PEG and PVP were absorbed into inner spaces, for which the adsorption capacity increased with molecular weight of the polymers. For Mt, all types of PEG could enter its micropores, while PVP with larger molecular weights appeared to be confined externally, leading to a decrease in the adsorption capacity of PVP with increasing molecular weight. The findings of this study provide a theoretical basis for scientific evaluation of environmental processes of WSPs.

1. Introduction

Currently, the environmental exposure and risk assessment of synthetic polymers has attracted considerable research attention. However, unlike water-insoluble plastic particles like microplastics (MPs) under the spotlight, little attention has been paid to the environmental exposures and risks of water-soluble polymers (WSPs) [2]. Common WSPs are a complex and diverse group of compounds, examples of them include polyethylene glycol (PEG), polyvinyl pyrrolidone (PVP), polyethylene oxide (PEO), polyvinyl alcohol (PVA), polycationic salts (PQs), polyacrylamide (PAM) and polyacrylic acid (PAA) [10,11,15]. WSPs play a vital role in human society, occupying the three highest value markets (personal care and cosmetics, agricultural chemicals and household cleaning products) with over 36.3 million tons produced globally each year, and the demand is expected to grow in the future [41]. WSPs of varying molecular weights are extensively employed. For example, PEG with lower molecular weights is used as a solvent, co-solvent, emulsifier, and stabilizer in applications like cement suspensions, emulsions, and injections [3]. Additionally, a study indicates that varying molecular weights of PAM showed diverse impacts when used as flocculants and high molecular weight PAM (> 10 kDa) possesses high viscosity, drag reduction capabilities, and moisture retention properties, making it widely applicable [44]. Inevitably, WSPs can enter the environment, and present in rivers, lakes, soil, sediments, and oceans [41]. Currently, there is increasing attention on assessing pollution levels, environmental fate, and risks associated with WSPs.

Research has shown that microplastics pose significant potential risks to aquatic environments, impacting the organic carbon cycle and water quality in water bodies [8]. However, there is scarce research on the aquatic behavior of WSPs. Nevertheless, the pollution levels of WSPs in aquatic environments are significant enough to warrant our attention. For instance, PEG 550 (number indicates average molecular weight) were found in river water and seawater at concentrations ranging between 0.5 and 68 μg/L [16,39]. Even studies have indicated that the concentration of PEG in wastewater treatment plants can be as high as 10–100 mg/L [15], and the concentration of PVP in river water affected by municipal sewage emissions has been reported to be around 0.1 mg/L [1]. The toxicity of micro- and nano-plastics has been extensively investigated, with examples such as PS-NPs disrupting the normal physiological functions of aquatic algae through mechanisms such as photosynthesis inhibition and induction of oxidative stress [49]. However, research on the toxic effects of WSPs remains limited. The existing studies indicated that anionic WSPs, such as PAA and PAM, predominantly affect aquatic species through constrained sorption, resulting in physical alterations rather than direct toxicity. PAA can hinder root growth in aquatic plants and potentially cause algal aggregation [37]. Besides, cationic WSPs, such as quaternized dimethylaminopropyl-acrylamide and acryloyloxydodecylpyridinium bromide, due to its high charge density, were reported to disrupt cell membranes and affect organisms at different trophic levels [26]. The biotoxicity of these polymers was also correlated with environmental factors, such as molecular weight, charge type, reactive functional groups, environmental factors [41,49]. Overall, these polymers pose complex ecological challenges and their effects vary based on their properties and environmental conditions. Therefore, scientific assessment of the environmental behavior of WSPs is crucial.

The interactions between WSPs and environmental components can significantly influence the transport and fate of WSPs [2]. An early study

first investigated the adsorption of PEG and PEI on sediments (R. Thomas [35]). The adsorption capacity of PEG on sediments increased with the increase in molecular weight; PEI, due to its cationic nature and higher cationic charge density, exhibited higher adsorption than PEG (R. Thomas [35]). As important components of sediments and soils, clay minerals are significant for environmental processes of a wide range of contaminants including organic pollutants and heavy metals [22,35]. Studies found that polymers such as PAM and PEO were capable of adsorbing on the surfaces of clay minerals (e.g., montmorillonite and kaolinite) via hydrogen bonding, thereby reducing their ability to migrate in the environment [19,5]. Understanding the interaction between WSPs and minerals is crucial for comprehending their transport and fate in environment. Nevertheless, there are only a limited number of relevant studies available, and the multiple interactions of their adsorption on minerals remain unknown, and this hinders our understanding of the overall fate and impact of WSPs in ecosystems.

The main objective of this study was to explore the interaction between WSPs and minerals. PEG and PVP were chosen as representative WSPs owing to their extensive range of applications. The interactions between PEG/PVP and minerals were systematically investigated using batch adsorption experiments. Fourier-transform infrared (FTIR) spectroscopy, Two-Dimensional Correlation Spectroscopy(2D-COS), X-ray powder diffraction (XRD), and other characterization methods were applied to reveal the intrinsic interaction mechanisms. The outcomes of this research not only contribute to the current understanding of the interactions between PEG/PVP and minerals, but also serve as a valuable reference for further migration and transformation of WSPs.

2. Materials and methods

2.1. Materials

Kaolinite and montmorillonite powders were purchased from Shanghai Acmec Biochemical Co., Ltd, China (labeled as Kaol and Mt respectively). Considering factors such as commercial availability, common industrial molecular weights, and research objectives, PEG and PVP with various molecular weights, including PEG:2 kDa, 6 kDa, 10 kDa, and PVP:10 kDa, 58 kDa, 1300 kDa, were also purchased from Shanghai Acmec Biochemical Co., Ltd, China. PEG and PVP stock solutions of 2 g/L was prepared by dissolving 0.04 g of PEG and PVP in 20 mL of ultrapure water (18.25 MΩ·cm), filtrated using a 0.45 μm pore size filter and then stored at 4 °C in a refrigerator before use. The six samples were denoted in order of decreasing molecular weight as "PVP-1″, "PVP-2″, "PVP-3″ and "PEG-1″, "PEG-2″, "PEG-3″, respectively. Use a TOC analyzer (TOC-L, Shimadzu) to measure the total organic carbon (TOC) value of a 2 g/L stock solution. The recorded TOC values were as follows: PVP-1: 1.09×10^3 mg/L, PVP-2: 1.13×10^3 mg/L, PVP-3: 1.10×10^3 mg/L, PEG-1: 1.05×10^3 mg/L, PEG-2: 1.03×10^3 mg/L, and PEG-3: 1.04×10^3 mg/L. All materials and chemicals were employed in original condition.

2.2. Adsorption experiments

The interaction between PEG/PVP and minerals was studied by batch adsorption experiments. For the adsorption kinetic experiment, 10 mL solutions of "PVP-1", "PVP-2", "PVP-3", "PEG-1", "PEG-2", and "PEG-3" were prepared in brown glass vial, with a concentration of 40 mg TOC/L. Simultaneously, prepared a sufficient volume of 20 mM NaCl

solution. Afterwards, blended the two solutions in equal volumes, which made the reaction volume 20 mL and the adsorbate TOC concentration 20 mg/L with an ionic strength of 10 mM, adjusting the pH to be within the range of 7 $\pm$ 0.2 through the careful addition of HCl and NaOH solutions (0.1 mM). Finally, individual glass vials were filled with 0.002 g of Mt or 0.1 g of Kaol with concentrations set at 0.1 g/L and 5 g/L, respectively. After measurement, there was minimal change in the pH value. Multiple brown glass vials containing this mixture were agitated in a temperature-controlled oscillator (HZQ-X500C, Bluepard, Beijing) at 25 °C and 150 rpm. At specific time intervals of 1 min, 5 min, 30 min, 1 h, 3 h, 5 h, 9 h, and 12 h a set of vials were taken out for subsequent analysis. The samples were filtrated using a 0.45 μm pore size filter to remove the minerals from the suspension. Then, 15 mL of supernatant was taken cautiously to measure the TOC concentrations of PEG and PVP using a TOC analyzer. The experiment was repeated twice for each group.

In the adsorption isotherm experiment, same amounts of adsorbents (0.05 g Mt or 2.5 g Kaol) were added to 500 mL glass vials containing PEG and PVP solutions at 2, 5, 10, 15, 20, 30,50 and 70 mg TOC/L. After shaking 24 h when they reach adsorption lequilibrium, the solution samples were filtrated using a 0.45 μm membrane filter and then 15 mL of supernatant was removed for detection. Each group was repeated twice. The detailed information of the Langmuir and Freundlich adsorption models is described in Text S1.

To investigated the impact of pH on adsorption, a series of adsorption experiments were conducted at varying pH levels. The pH values of the solution were adjusted to 3, 5, 7, 9 and 11 using NaOH and HCl. Each glass vial received 0.25 g of Kaol or 0.05 g of Mt, and 500 mL of PVP-1 or PEG-1 solution at a concentration of 20 mg/L, 20 samples in total. Glass vials were placed in a thermostatic oscillator and shaken at 25 °C at 150 rpm for 24 h. Subsequently, the samples were collected for analysis. Each group had two parallel samples as a reference.

2.3. FTIR and 2D-COS analysis

FTIR Spectrometry (Nicolet iN10MX, Thermo Fisher Scientific) was employed to monitor PEG/PVP with different molecular weights and their interactions with minerals at various concentrations in the conditions of a scan range of 500–4000 cm^{-1} and resolution of 8 cm^{-1}. Two-dimensional correlation spectroscopy (2D-COS) analysis was applied to investigate the sources of small variations in the infrared peaks of the samples, using Origin 2021 software (Northampton, Massachusetts, USA). All FTIR spectra were normalized, baseline-corrected and denoised by OMNIC. More details of the 2D-COS analysis are provided in Text S2.

2.4. Characterization of PEG, PVP and minerals

For minerals, scanning electron microscopy (SEM, Quattro, FEI, Czech Republic) was used to characterize the morphologies and physical dimensions. The determination of mineral surface areas was accomplished via N$_2$ adsorption/desorption isotherms, utilizing Micromeritics ASAP 2460. Additionally, BET analyses were conducted, employing the HK and BJH models for pore size and distribution characterization on the surfaces of the two minerals. For WSPs, we utilized dynamic light scattering (DLS, ZS90, Malvern Instruments Limited, UK) to measure the hydrodynamic size of PEG and PVP with varying molecular weights and concentrations. The DLS was also applied to ascertain the point of zero charge (PZC) for both minerals and WSPs. For both minerals and PEG/PVP mixtures, the residue remaining after removing the supernatant from the above adsorption experiments was dried at 45° and then subjected to characterization. The crystal structure of minerals before and after adsorption was determined utilizing X-ray powder diffraction (XRD, X'Pert 3 powder, PANalytical, Netherlands). Furthermore, FTIR spectroscopy were conducted to analyze possible binding sites for elucidating the binding mechanisms of PEG/PVP and minerals, with 2D-

COS analysis being employed to discern subtle spectral variations.

3. Results and discussion

3.1. Characteristics of WSPs and minerals

In terms of minerals, the SEM images (Fig. 1e, f) showed that Mt exhibited a flaky structure, while Kaol appeared blocky with a slightly hexagonal arrangement. Both displayed an irregular surface dotted with numerous small holes. Nitrogen BET measurements for the minerals revealed that the specific surface areas were 12.3 m^2/g for Kaol and 75.4 m^2/g for Mt. As shown in zeta potentials measurements (Fig. 1c), both Kaol and Mt exhibited a negative surface charge (< -17 mV), which became more negative as the pH increased. The particle sizes of Kaol and Mt were determined to be 2.14×10^3 nm and 5.54×10^3 nm, respectively (Table S1), in concordance with the SEM observations. From FTIR spectroscopy analysis (Fig. S1), the peak at 540 cm^{-1} corresponded to Si-O-Al vibrations in Kaol [52], 1072 cm^{-1} was related to the Si-O vibration within the vertical layer [12]. For Mt, the peaks was attributed to the Mg(Al)-OH bending vibration and the Si-O-Si asymmetric stretching vibration were observed at 973 cm^{-1} [42]. The peaks at 810 and 3616 cm^{-1} corresponding to Al-OH bending vibrations [4].

Regarding WSPs, the average size distributions of PEG and PVP with different molecular wight in the NaCl solution (pH 7, 10 mM) were ascertained via DLS measurements (Fig. 1d). Notably, particle size of all WSP samples were not detectable at the experimental concentration (20 mg TOC/L) levels. Consequently, high-concentration samples were prepared to facilitate the observation of the particle size distribution. The results unveiled that for PVP-1, the hydrodynamic diameters (Dh) were 26.8 nm, 39.2 nm and 42.6 nm at concentrations of 10 g/L, 2 g/L, and 1 g/L, respectively. For PVP-2, the Dh values were 11.1 nm, 17.8 nm and 8.38 nm, respectively. However, no measurable size was observed for PVP-3. Similarly, for all molecular weights PEG dissolved in NaCl solution, Dh could not be measured, possibly owing to the small molecular weights of PEG falling below the instrument's detection limit, even at higher concentrations. Notably, the Dh measurements of PVP might not directly represent the actual size of PVP molecules in the adsorption experiments, but the results provided some information on possible size range of PVP with different molecular weight. Zeta potentials (ZP) of PEG and PVP with varying molecular weights at different solution pHs were depicted in Fig. 1c. The ZP of all tested PVP and PEG remained approximately neutral as the pH increased from 2.0 to 11.0, indicating that the PEG and PVP were uncharged.

FTIR spectroscopy was performed to analyze the functional groups of different molecular wight PEG and PVP. It could be inferred that the molecular weight of neither PVP nor PEG significantly affected their respective functional groups. For PVP (Fig. 1a), the absorption peak at 2951 cm^{-1} arose from the C-H asymmetric stretching vibrations [38]. A prominent peak at 1654 cm^{-1} represented the C=O stretching vibration absorption, while the absorption peak at 1277 cm^{-1} was attributed to the combined effects of C-N stretching and N-H bending vibrations. Additionally, absorption peaks at 1373 cm^{-1} and 1428 cm^{-1} were due to the C-H asymmetric deformation and scissoring vibrations, respectively [21,29]. For PEG (Fig. 1b), peaks at 2861 and 1341 cm^{-1} were ascribed to the C-H symmetric stretching vibration and out-of-plane wagging vibration, respectively [36]. The split double peak at 1454 cm^{-1} was attributed to the C-H bending vibration, while the C-H rocking vibration mode was observed at 841 cm^{-1} [50]. The strong peaks at 1095 cm^{-1} was due to the presence of C–O–C structure [25].

3.2. Adsorption behavior of PEG and PVP on minerals

3.2.1. Adsorption kinetics

The adsorption kinetics of the PEG and PVP on minerals are shown in Fig. S2. Generally, Mt exhibited higher adsorption capacity towards PEG and PVP than Kaol, which may be attributed to its expansive specific
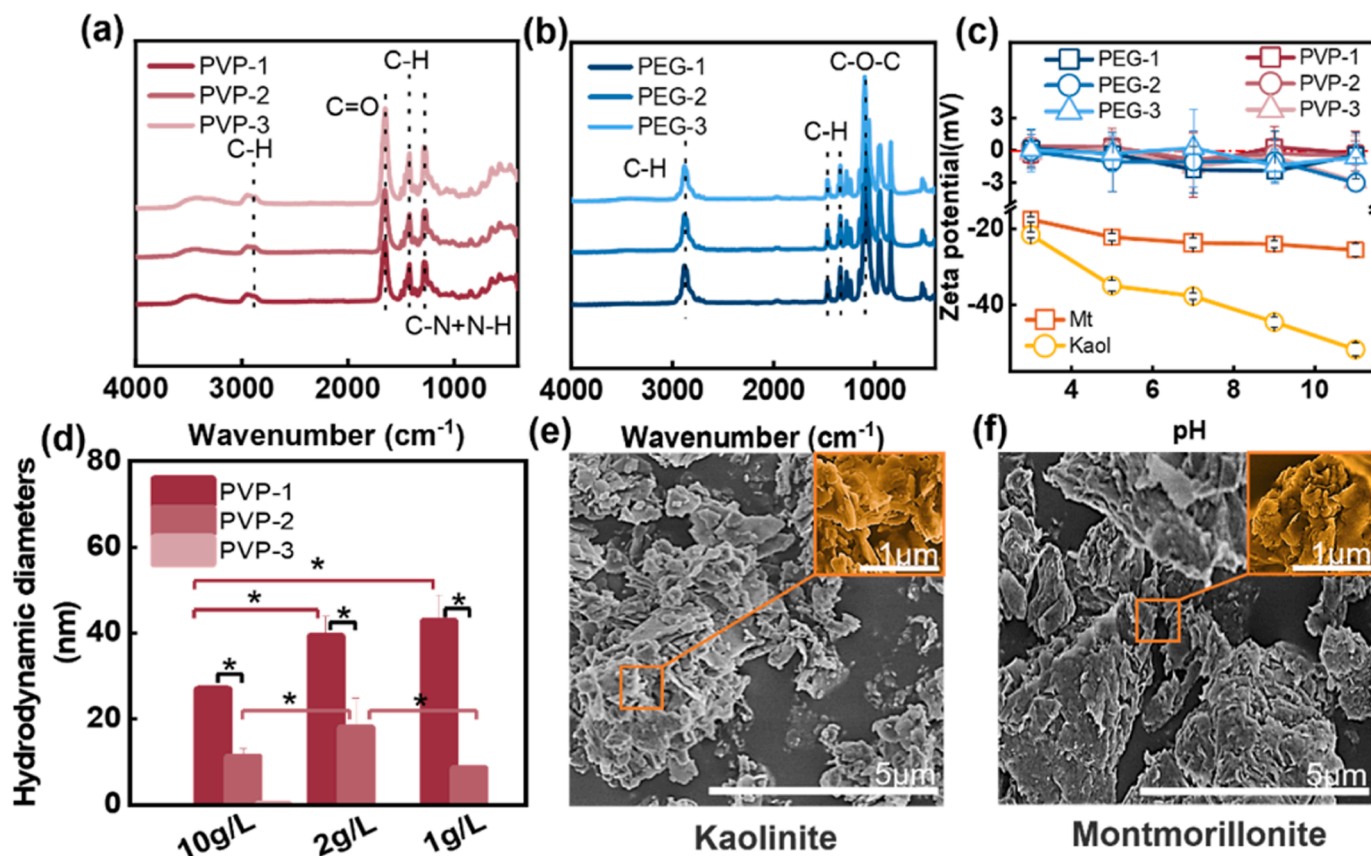
Fig. 1. (a) FT-IR Spectra of PVP with different molecular weights, (b) FT-IR Spectra of PEG with different molecular weights, (c) Relationship between Zeta potential and solution pH, (d) Effect of solution concentration and molecular weights on hydrodynamic diameter of PVP, * : There is a significant difference between the two data sets, $p < 0.05$, (e, f): SEM images of two minerals.

surface area. Equilibrium adsorption was achieved within a relatively short timeframe, typically between 0.5 to 2 h. The adsorption kinetic parameters are presented in Table S2. For the pseudo-first-order reaction kinetic model, the rate constant K_1 and the calculated equilibrium capacity ($q_{e\ cal}$) were determined from the slope and intercept of the ln (q_e-q_t)-t curve [45]. However, on minerals, the calculated equilibrium adsorption capacity ($q_{e\ cal}$) did not exactly match the experimental equilibrium capacity ($q_{e\ exp}$). Moreover, from the fitting results for PVP, the R^2 values for the pseudo-first-order kinetic model were generally lower than the R^2 values for the pseudo-second-order kinetic model (>0.99), indicating that the pseudo-second-order kinetic model could accurately simulate its adsorption on minerals. In contrast, this was exactly the opposite for PEG.

As observed (Table S2), on Kaol PVP and PEG with smaller molecular weights exhibited larger fitted K values, indicating higher adsorption rates. This was because smaller molecular sizes led to faster diffusion during the initial adsorption processes [18]. However, WSP with larger molecular weights exhibited faster adsorption on Mt, which might be related to the large specific surface area and pore structure of Mt. For instance, larger molecular WSPs might quickly adsorb on the external surface of Mt and reach saturation, while WSPs with smaller molecules could partially adsorbed at internal pore sites (see analysis in Section 3.4.2), gradually reaching equilibrium. Notably, the adsorption rate of PVP (10 kDa) on Kaol was greater than that of PEG (10 kDa), which is likely due to their difference in molecular structure. PVP with both hydrophobic and hydrophilic segments might possess short cross-linked cyclic structures [13] while hydrophilic PET likely exhibited the long linear structure that might hinder surface diffusion [31]. On Mt, the adsorption rate of PVP was smaller than that of PEG because the minimum molecular size of PEG was smaller than that of PVP, which might

make it easier for PEG to diffuse into the mesopores of Mt (Fig. 4a, b) [30]. When examining the equilibrium concentrations (q_e) for PEG or PVP individually, it was generally observed that WSPs with higher molecular weights were associated with increased adsorption capacity on two minerals, possibly due to enhanced van der Waals interactions [23]. Under the same molecular weight and initial concentration conditions, the q_e values for PVP-3 (10 kDa) on Kaol and Mt were 2.88 mg/L and 147 mg/L, respectively, approximately twice that of PEG-1 (10 kDa, 1.32 mg/L, 65.3 mg/L), indicating that PVP was more prone be adsorbed by minerals.

3.2.2. Adsorption isotherms

Fig. 2 presents the adsorption isotherms of PEG and PVP (different molecular wights) onto minerals, with corresponding model parameters summarized in Table 1. The data aligned well with the two models, as indicated by the R^2 value. The Langmuir model-derived q_m values revealed that the adsorption capacities of PEG on Kaol, listed in descending order of molecular weight, were 1.80, 0.935, and 0.576 mg/L, respectively. The adsorption capacities of PEG on Mt were significantly higher, with q_m values of 102, 54.8, and 21.7 mg/L, respectively. A positive correlation between adsorption capacity and molecular weight of PEG was observed in both minerals. In contrast, for PVP on Kaol, when the molecular weight was relatively large (> 58 kDa), there was essentially remained unchanged in its adsorption capacity, ranging from 7.68 mg/L to 8.47 mg/L. This suggested that the impact on adsorption became minimal once the molecular weight reached a certain threshold. Interestingly, the adsorption behavior of PVP on Mt was completely opposite. As depicted in Fig. 2b, the adsorption capacity of PVP on Mt exhibited a negative correlation with its molecular weight. Specifically, a PVP with a molecular weight of 1300 kDa yielded an
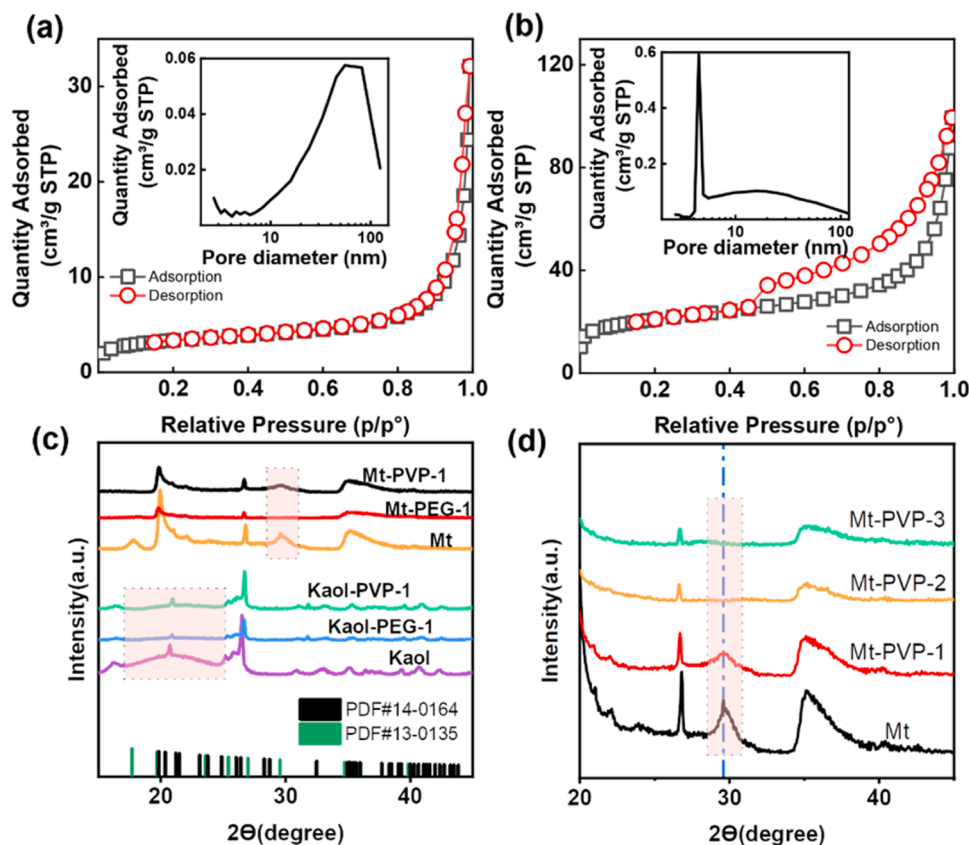
Fig. 4. BET isotherms and corresponding pore size distributions. (a: Kaolinite); (b: Montmorillonite), (c) XRD Patterns of minerals before and after adsorption of PEG-1 and PVP-1, (d) XRD Pattern of montmorillonite after adsorption of PVP with different molecular weights.

adsorption capacity of merely 60.0 mg/L, whereas a 10 kDa PVP demonstrated a significantly higher capacity at 273 mg/L.

It is known that the Langmuir model is greatly limited in practical situations, as it does not account for interactions between adsorbates [6]. In contrast, the Freundlich model, which assumes multilayer adsorption, is more universal [43]. The adsorption of PEG and PVP was likely to occur on the heterogeneous surface of minerals. In general, when the $1/n$ value of the Freundlich model fitting approached 1.0, the adsorption process was more uniform. Within our study, the Freundlich model's $1/n$ values were significantly below 1.0, indicating limited adsorption sites and competition between PEG and PVP of different molecular weights [20]. As the molecular weight of PVP increased, its $1/n$ values decreased on both Kaol and Mt, indicating that larger molecular weight PVP exhibited stronger competition for adsorption sites. While PEG behaves differently, with its $1/n$ value increasing as the molecular weight increased. On the one hand, smaller molecular weights could easily occupy adsorption sites due to their smaller size and shorter chains. On the other hand, compared to PEG, PVP had a larger molecular weight (PEG < 10 kDa, PVP > 10 kDa), which allowed PVP to interact with multiple sites on the Kaol and Mt surface during the adsorption process, thereby enhancing competition. On Mt, the $1/n$ value for PEG was consistently lower than that of PVP (with a maximum value of 0.342 for PEG and a minimum value of 0.433 for PVP), while this pattern did not hold on Kaol, and the deviation could indeed stem from the influence of the specific pore structure on the mineral surface. With regard to the same mineral, the k_f value of PEG-1 was 25.5 $(mg·g^{-1})/(mg·L^{-1})^n$ and 0.514 $(mg·g^{-1})/(mg·L^{-1})^n$ on Mt and Kaol, respectively, compared to 12.1 $(mg·g^{-1})/(mg·L^{-1})^n$ and 0.295 $(mg·g^{-1})/(mg·L^{-1})^n$ for PEG-3 (Table 1), the adsorption affinity (k_f) of PEG-1 was substantially higher than that of PEG-3. This indicated that PEG of higher molecular weight exhibited a greater propensity for mineral adsorption. Similarly, PVP adsorbed on Kaol meted this trend.

3.3. FTIR spectra and 2D-COS analysis

The FTIR spectra of PVP-Mt, PEG-Mt, PVP-Kaol and PEG-Kaol (Fig. S3) were further used to identify the binding sites. For Mt (Fig. S3a, c), the adsorption of both PEG and PVP on its surface shares several common characteristics. For example, Mg(Al)-OH and Si-O-Si was observed and the band intensity increased with the adsorption molecular weights, peaks at 810 and 3616 cm^{-1} were due to Al-OH bending vibrations, exhibited a gradual broadening and reduction in intensity as the molecular weight decreased. This effect was particularly pronounced in the case of PVP adsorption on Mt. It was noteworthy that peaks at 1629 and 3382 cm^{-1} were unchanged during the adsorption process for PEG on Mt. While, after the adsorption of PVP, the peak (H-O-H) shifted from 1629 cm^{-1} to 1646 cm^{-1} and its peak intensity increases as the molecular weight decreased, indicating that the unique C=O bond in PVP exerted an influence on the adsorption. Furthermore, under the influence of the C-N bonds in PVP, a strong new peak was also observed at 1277 cm^{-1}. Meanwhile, as shown in Fig. S3a, c, new peaks also appeared at approximately 1428 and 2951 cm^{-1}, implying that the C-H bond of PEG and PVP might interact with the surface functional groups of Mt at this particular location [9] and the intensity of the new peak was consistent with the adsorption rules of PEG and PVP on Mt as described in the adsorption experiments.

The spectral changes after the adsorption of PEG/PVP on Kaol were essentially consistent with the changes observed when they were adsorbed on Mt. The FTIR spectrum underwent more pronounced changes after the adsorption of PVP (Fig. S3 d), indicating that the PVP had stronger adsorption capacity than PEG on Kaol. In contrast, after PEG adsorption, the peaks at 1629 and 3382 cm^{-1} occurred, which might be attributed to the -OH groups generated when PEG dissolves in water, which meant -OH also played a positive role in the adsorption process. In addition, peaks at 540 cm^{-1} belonged to Si-O-Al vibrations
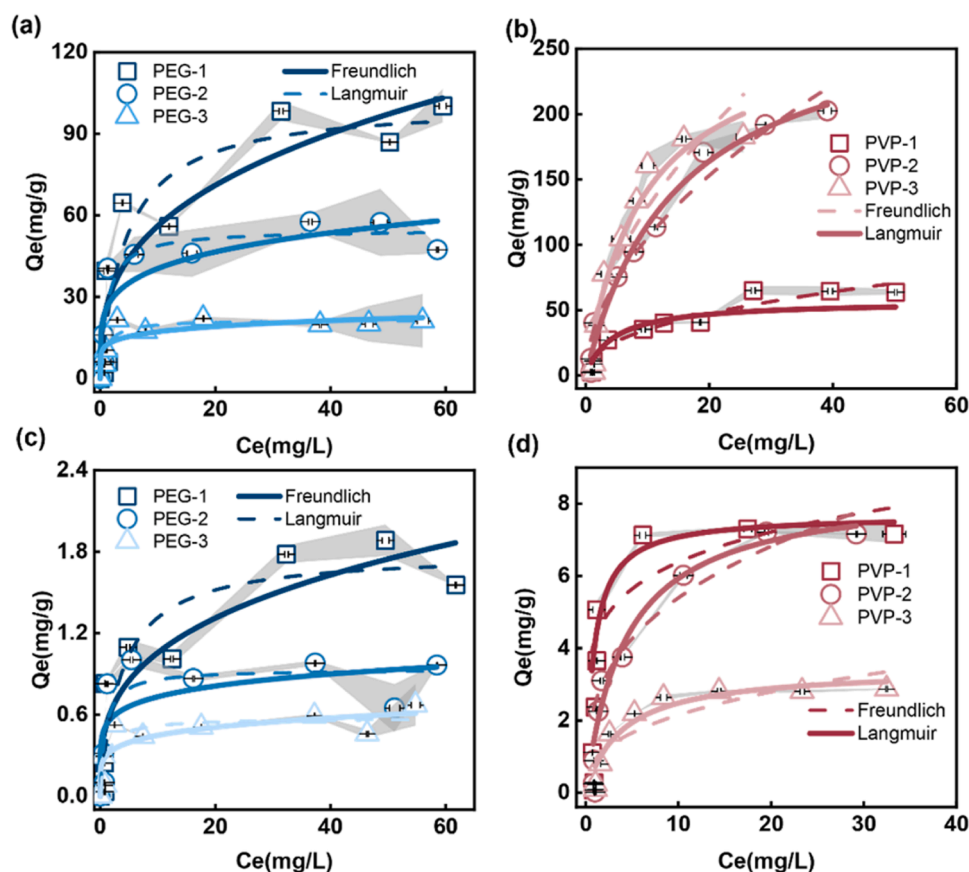
Fig. 2. Adsorption isotherms of the PEG and PVP to minerals with the shaded areas indicating the error bars. (a, b: montmorillonite; c, d: kaolinite).

Table 1
Fitted parameters of the adsorption isotherm.

Adsorbents	Adsorbates	Molecular weight (kDa)	Langmuir model			Freundlich model		
			q_m	K_L	R^2	$1/n$	K_F	R^2
Kaol	PVP	1300	7.68	1.17	0.997	0.178	4.24	0.994
		58	8.47	0.234	0.998	0.339	2.47	0.996
		10	3.44	0.259	0.999	0.376	0.905	0.998
	PEG	10	1.80	0.273	0.787	0.312	0.514	0.828
		6	0.935	1.11	0.541	0.148	0.520	0.563
		2	0.576	0.929	0.605	0.181	0.295	0.737
Mt	PVP	1300	60.0	0.229	0.999	0.433	13.0	0.913
		58	286	0.067	0.982	0.540	30.3	0.958
		10	273	0.108	0.928	0.549	36.4	0.840
	PEG	10	102	0.226	0.808	0.342	25.5	0.821
		6	54.8	0.806	0.801	0.203	25.3	0.777
		2	21.7	0.961	0.770	0.154	12.1	0.755

Note: the units of q_m (mg/g), K_L (L /mg), K_F (mg/g)/(mg/L)^n.

were unchanged during the adsorption process, but a peak at 1072 cm^{-1} associated with Si-O vibrations exhibited an intensity increase as both the molecular weight and concentration increased.

In conclusion, across all minerals, the presence of peaks at 1300–1500 cm^{-1}, attributed to C-H, was consistently observed. Notably, the intensity of these bands exhibited a direct correlation with the concentration of WSPs. In addition, spectral perturbations resulting from adsorption on Mt have been found to exceed those on Kaol, suggesting that more WSP was adsorbed on Mt.

To gain a more detailed understanding of the changes in functional group intensities of Mt and Kaol during adsorption, a 2D-COS analysis was conducted (Figs. 3, and S4). With varying PEG concentration, maximum intensity of the peak at 1095 cm^{-1} (C-O-C) was observed, followed by the peaks at 2861, 1454 and 1341 cm^{-1} (C-H). Based on

Noda's rules [27,28], the order of adsorption of PEG-1 on Mt was 1095 (C-O-C) > 1454 (C-H) > 2861 (C-H) > 1341 cm^{-1} (C-H). Similarly, the order of change in the functional group strength of PEG-2 and PEG-3 was 2816 (C-H) > 1341 (C-H) > 1454 (C-H) > 1095 cm^{-1} (C-O-C) (Fig. 3a-f, Tables S3, S4). The sequence indicated that during the adsorption process, the C-O-C bond in high molecular weight PEG-1 exhibited a stronger interaction with minerals. Conversely, for lower molecular weights, the C-H bond, specifically at 2816 cm^{-1}, played a more prominent role. Secondly, regarding the changes in the mineral peaks: the corresponding change order of PEG-1, PEG-2, PEG-3 was 973 (Mg (Al)-OH) > 3616 (Al-OH) > 3382 (H-O-H) > 1629 cm^{-1} (H-O-H), 973 > 3382 > 3616 > 1629 cm^{-1}, 3382 > 3616 > 1629 > 973 cm^{-1}, respectively (Table S3 and S4). The results showed that the metal hydroxyl bonds with hydration on the Mt easily interact with PEG.
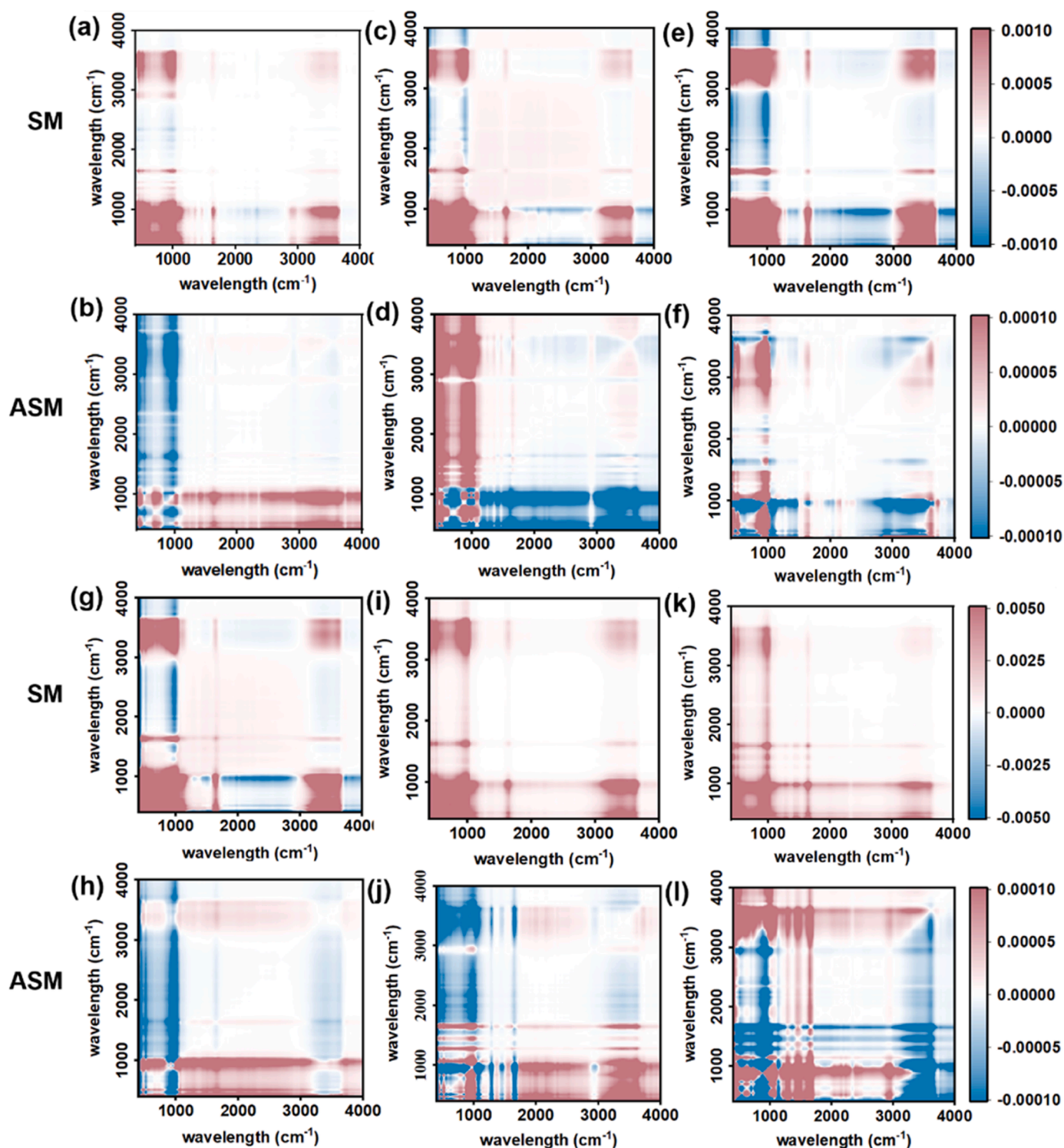
Fig. 3. Two-dimensional correlation spectrum of PEG and PVP on montmorillonite at different adsorption concentration. Red color indicates positive correlation, and blue color denotes negative correlation; deeper color demonstrates higher intensity and therefore stronger positive or negative correlation. (a, b) PEG-1; (c, d) PEG-2; (e, f) PEG-3; (g, h) PVP-1; (i, g) PVP-2; (k, l) PVP-3, SM: synchronization map; ASM: Asynchronous map.

For PVP-1 on Mt, negative cross peaks were observed at 1428/2951, 1277/1654, 1428/1654 cm^{-1} above the diagonals of the asynchronous map, with corresponding positions on the synchronous map being positive. These findings suggest that as the concentration of PVP-1 varied, the sequence was 1654 (C=O) > 1277 (C-N) > 2951 (C-H) > 1428 cm^{-1} (C-H). Similarly, the adsorption sequence for PVP-2 and PVP-3 on Mt was as follows: 1277 (C-N) > 1654 (C=O) > 1428 (C-H)

> 2951 cm^{-1}(C-H) and 2951 (C-H) > 1277 (C-N) > 1654 (C=O) > 1428 cm^{-1} (C-H), respectively (Fig. 3g-l and Tables S5, S6). The findings proposed that within the functional groups of PVP, the C=O and C-N groups assumed a crucial role in adsorption, potentially linked to the formation of hydrogen bonds with Si-O and Al-O groups on the mineral surface. Moreover, the C=O group, when associated with a larger molecular weight, exerted a more noticeable effect, while the C-N

group, when associated with a smaller molecular weight, exhibited a stronger influence. Regarding the changes in the mineral peaks, the order of PVP-1, PVP-2, PVP-3 were 973 (Mg(Al)-OH) > 3382 (H-O-H) > 3616 (Al-OH) > 1629 cm^{-1} (H-O-H), 1629 > 973 > 3382 > 3616 cm^{-1}, 3616 > 3382 > 973 > 1629 cm^{-1}, respectively (Tables S5, S6). We could observe that, for PVP of varying molecular weights, there existed a pronounced interaction with the metal hydroxyl bonds on the mineral surface, particularly with aluminum hydroxyl bonds.

According to the same analysis method mentioned above, the order of PEG-1, PEG-2 and PEG-3 interacting with Kaol was as follows: 1095 (C-O-C) > 1341 (C-H) > 1454 (C-H) > 2861 cm^{-1} (C-H); 1341 (C-H) > 1454 (C-H) > 2861(C-H) > 1095 cm^{-1} (C-O-C); 2861 (C-H) > 1454 (C-H) > 1341(C-H) > 1095 cm^{-1} (C-O-C); Meanwhile, the sequence of PVP-1, PVP-2, and PVP-3 adsorbed on Kaol followed the order of 1654 (C=O) > 2951 (C-H) > 1428 (C-H) > 1373 (C-N) > 1277 cm^{-1} (C-N); 2951 (C-H) > 1428 (C-H) > 1373 (C-H) > 1654 (C=O) > 1277 cm^{-1} (C-H); 2951 (C-H) > 1654 (C=O) > 1277 (C-N) > 1373 (C-H) > 1428 cm^{-1} (C-H) (Fig. S4 and Table S7-S10). As for mineral peaks, among all tested PEG and PVP, 1072 (Si-O) > 540 cm^{-1} (Si-O-Al). The results indicated that whether adsorbing PVP or PEG, the most pronounced alterations were observed in the mineral peak Si-O. Looking individually, the C-O-C had a significant role in adsorbing PEG with a large molecular weight. Simultaneously, the C=O bond exhibited more substantial changes when PVP with a high molecular weight was adsorbed. The more oxygen-containing functional groups, and the greater the binding force with minerals. In general, the adsorption sequence of PEG and PVP on minerals indicated that hydrogen bond force was the main adsorption mechanism. On Mt, the change in Al-O was the most intense and had a huge impact on adsorption, while on Kaol, the binding of WSPs with Si-O was stronger. For WSPs, there was a strong interaction between oxygen-containing functional groups and minerals when the molecular weight was larger, whereas alkanes became significant when the molecular weight was smaller.

3.4. Insight into the adsorption mechanism

3.4.1. Hydrogen bonding-dominant adsorption

The effect of solution pH on the adsorption of PEG and PVP (PEG-1, PVP-1) was examined over a pH range of 3 to 11 (Fig. S5). We found both Kaol and Mt were negatively charged, which was consistent with previous research [53]. For all minerals, the adsorption of PEG and PVP was only slightly pH dependent, but overall, the adsorption capacity was greater at lower pH values. Notably, the effects of pH on PVP-1 were strikingly different compared to those on Mt in the given pH range. For instance, the adsorption rates varied from 25% to 32% on Mt. As previously mentioned, PEG and PVP tested in this study were non-ionic polymers as the zeta potentials of PEG and PVP remained approximately zero in the given pH range. Therefore, the electrostatic interaction was not the dominant force in the adsorption, and the effect of pH on the adsorption was attributed to other forces.

Considering the intermolecular forces, van der Waals forces existed between WSPs and minerals, exerting a certain influence on adsorption. Typically, WSPs with high molecular weight contained longer polymer chains and more adsorption sites, which enhanced their adsorption and allowed them to simultaneously adsorb to multiple particle surfaces. For instance, linear chains of PAM with higher molecular weights was more effective bridging polymers, and thus showed stronger adsorption capacity [33]. FTIR spectra and 2D-COS results indicated that hydrogen bonding also played a key role in PEG/PVP adsorption process. Many functional groups in common organic pollutants could act as hydrogen bond donors and/or acceptors, as mentioned previously [34]. Even though the siloxanes on the surface of the substrate were only weak hydrogen bonding acceptors, the formation of hydrogen bonds might be facilitated by polar functional groups such as amides, ester carbonyls, carboxyls, carbonyls, and amines [17]. Besides, diverse cations were

found on the clay mineral edges, such as Ca^{2+}, Mg^{2+}, H^+, Na^+, and Al^{3+}. These groups not only bridged hydrogen bonds between minerals and organic or inorganic molecules, but also combined with water, which pumped out electrons, making them powerful hydrogen bond donors [24,32,46]. In this study, Si-O and Al-O on minerals could act as H-bond donors and acceptors. The C-N and C=O bonds in PVP, along with the C-O-C bonds in PEG, were more inclined to facilitate the formation of hydrogen bonds on mineral surface. The larger adsorption of larger molecular weights may also be related to these polar functional groups being more likely to form hydrogen bonds. Similarly, the hydrogen bonds formed between the amide and ether oxygen functional groups of PAM and PEO, and aluminate groups on the minerals, has been identified as crucial for the adsorption of these polymers [19,5]. The presence of hydrogen bond also explained the increased adsorption of aged polystyrene nanoplastics (PS NPs) on minerals compared to pristine NPs, as the aging process led to the formation of additional oxygen-containing functional groups [51].

As reported, Van der Waals forces demonstrated low sensitivity to changes in solution chemistry, such as variations in ionic strength and pH [14]. However, it was important to note that pH does influence hydrogen bonding [14]. An increase in pH could result in the deprotonation of oxygen-containing functional groups and reduced the availability of hydrogen-bond donors, weakening the hydrogen bond interactions [7]. In the context of this study, a lower pH resulted in the protonation of functional groups on the mineral surfaces, facilitating the formation of hydrogen bonds between WSPs and minerals. All in all, the adsorption of PEG and PVP on minerals was dominated by hydrogen bonding.

3.4.2. Synthetic effect of molecular weight of WSPs and pore size of minerals

To further elucidated the impact of pore size and distribution on mineral surfaces on the adsorption behavior of two WSPs, we performed BET analysis on our samples. The N_2 adsorption-desorption isotherms of the two clay minerals are presented in Fig. 4a, b. According to the International Union of Pure and Applied Chemistry chemical nomenclature (IUPAC) classification [40], the isotherm of Kaol resembled type II with hysteresis at $0.823 < P/P0 < 0.981$, while Mt belonged to type IV with H3 hysteresis loops. The results of the HK model analysis showed that the micropore size distribution curves of both were narrow and centered at 1 nm, with no significant difference (Fig. S6). In contrast, a marked discrepancy was observed in the distribution of mesopore sizes. According to the BJH model, the pore diameter of Kaol predominantly ranged from 70–90 nm, whereas that of Mt was approximately 3 nm. Consequently, for PEG with relatively small molecular weights (<10 kDa), they could freely permeate the mineral interior and adhere to the principle of both Kaol and Mt. As the molecular weight increased, the adsorption capacity of PEG on two minerals tended to increase. Similarly, the adsorption capacity of PVP on Kaol also increased with the increase in the molecular weight as all forms of PVP were able to penetrate the micropores of Kaol effectively. In contrast, the molecular weights of PVP-1 were larger (>58 kDa), exceeding the mesopore diameter of Mt, which restricted their adsorption to the inner surface of Mt. This explained why an increase in the molecular weight of PVP resulted in a decrease in its adsorption.

In order to further verified the important effects of pore diameter, we used X-ray diffraction (XRD) to observe changes in the crystal structure of minerals. The X-ray diffraction patterns were shown in Fig. 4c, and characteristic reflection agreed with the standard ICDD (International Center for Diffraction Data) reference patterns for Kaol (PDF No. 14–0164) and Mt (PDF No. 13–0135), respectively [47,48]. After PEG/PVP adsorption, all reflections were clearly identified (Fig. S7), meanwhile changes occurred. For Kaol, compared to the original structure diagram, the intensity peak at 20° became narrower and sharper after all texted WSPs adsorption, which indicated that the crystallinity was improved. Based this, it could be concluded that PEG

and PVP had enough power to enter into the interlayer space of Kaol. In contrast, the crystallinity change of Mt was larger than that of Kaol. The disappearance of the 30° peak was likely attributed to the insertion of PEG into the interlayers, altering the crystalline structure. As shown as Fig. 4d, the adsorption of PVP-2 and PVP-3 on Mt induced the disappearance of the 30° peak in the X-ray diffraction pattern, while PVP-1 did not significantly change the crystal structure of Mt. This indicated that PVP-1 was adsorbed on the surface but both PVP-2 and PVP-3 had the ability to infiltrate the interior of Mt. Regarding the adsorption capacity of PVP on Mt, it was proposed that PVP-1 with the largest molecular weight was completely confined to the external surface of the Mt. In contract, PVP-3 with the smallest molecular weight demonstrated a superior capacity to penetrate the interior of Mt compared to PVP-2.

Meanwhile, significant differences were observed in the adsorption of solid plastics and "liquid plastics" we studied. The adsorption capacity and affinity of PS NPs on clay minerals were found to be much lower than those of all experimental molecular weights of PEG/PVP (mg/kg vs mg/g) [51]. Although electrostatic repulsion due to the negative charge of PS NPs might explain this difference, the disparity in size distribution between PS NPs and WSPs might also play a critical role. PS NPs, characterized by an average particle size of 50 nm [51], might partially penetrate the interior of Kaol but tend to be confined to the external surface of Mt, which can also explain the lower adsorption of NPs compared to WSPs due to reduced availability of binding sites on minerals. Therefore, due to the hydrophilic nature and lower molecular weight of liquid plastics, they may exhibit distinct environmental behaviors and associated risks when compared to solid plastics.

4. Conclusions

Increasing attention has been focused on the potential environmental risks and impacts of WSPs. Currently, research on WSPs is in its initial stages, articles related to environmental processes are scarce. In this article, we first studied the adsorption of "liquid plastics" and revealed the reaction mechanism. The results showed that Mt had a stronger adsorption capacity than Kaol, approximately 100 times higher. Whether it was PEG or PVP, when the molecular weight was less than 58 kDa and could enter the pores on the mineral surface, the adsorption capacity on minerals was proportional to the molecular weight. Adsorption behavior can be explained by hydrogen bonding and van der Waals forces. WSPs with larger molecular weights had stronger van der Waals forces, which promoted mineral adsorption. Furthermore, FTIR spectra and 2D-COS analysis indicated that Al-O and Si-O were important binding sites for the adsorption of PEG and PVP. The polar functional groups, such as C-O-C on PEG and C-N, C=O on PVP, facilitated hydrogen bond formation, especially for larger molecular weight PEG and PVP. This research contributes to understanding the environmental fate of WSPs, allowing us to better address issues related to environmental quality and ecosystem health. However, the properties of WSPs depend on their molecular weight and charge, leading to various applications. This study only focused on non-ionic WSPs, and the interactions between ionic WSPs and clay minerals in environmental processes remain unknown. And this work aimed to uncover the reaction mechanisms between WSPs of different molecular weights and minerals, with limited exploration of other environmental influencing factors. Additionally, WSP adsorption may alter the structure of minerals, potentially affecting the adsorption and migration processes of other environmental pollutants. All these topics require further research and exploration.

CRediT authorship contribution statement

Liu Gang: Writing – review & editing, Supervision, Resources, Methodology, Funding acquisition, Conceptualization. **van der Meer Walter:** Writing – review & editing, Supervision, Funding acquisition. **Chen Wenwen:** Writing – review & editing, Supervision. **Ou Qin:** Methodology, Investigation. **Xu Yanghui:** Writing – review & editing, Writing – original draft, Methodology, Investigation, Conceptualization. **wang Xintu:** Writing – review & editing, Writing – original draft, Methodology, Investigation, Formal analysis, Conceptualization.

Declaration of Competing Interest

The authors declare that they have no known competing financial interests or personal relationships that could have appeared to influence the work reported in this paper.

Data availability

Data will be made available on request.

Environmental implication

The findings of this study provide a theoretical basis for scientific evaluation of environmental migration and transformation fate of water-soluble polymers in the solid-liquid system, and it is conducive to our discovery of the potential hazards of water-soluble polymers.

Appendix A. Supporting information

Supplementary data associated with this article can be found in the online version at doi:10.1016/j.jhazmat.2024.133592.

References

[1] Antić, V.V., Antić, M.P., Kronimus, A., Oing, K., Schwarzbauer, J., 2011. Quantitative determination of poly(vinylpyrrolidone) by continuous-flow off-line pyrolysis-GC/MS. J Anal Appl Pyrolysis 90 (2), 93–99. https://doi.org/10.1016/j.jaap.2010.10.011.

[2] Arp, H.P.H., Knutsen, H., 2020. Could We Spare a Moment of the Spotlight for Persistent, Water-Soluble Polymers? Environ Sci Technol 54 (1), 3–5. https://doi.org/10.1021/acs.est.9b07089.

[3] Bernhard, M., Eubeler, J.P., Zok, S., Knepper, T.P., 2008. Aerobic biodegradation of polyethylene glycols of different molecular weights in wastewater and seawater. Water Res 42 (19), 4791–4801. https://doi.org/10.1016/j.watres.2008.08.028.

[4] Bhattacharyya, K.G., Gupta, S.S., 2008. Adsorption of a few heavy metals on natural and modified kaolinite and montmorillonite: a review. Adv Colloid Interface Sci 140 (2), 114–131. https://doi.org/10.1016/j.cis.2007.12.008.

[5] Bolto, B., Gregory, J., 2007. Organic polyelectrolytes in water treatment. Water Res 41 (11), 2301–2324.

[6] Cai, L., Wang, J., Peng, J., Wu, Z., Tan, X., 2018. Observation of the degradation of three types of plastic pellets exposed to UV irradiation in three different environments. Sci Total Environ 628-629, 740–747. https://doi.org/10.1016/j.scitotenv.2018.02.079.

[7] Chen, W., Qian, C., Liu, X.Y., Yu, H.Q., 2014. Two-dimensional correlation spectroscopic analysis on the interaction between humic acids and TiO2 nanoparticles. Environ Sci Technol 48 (19), 11119–11126. https://doi.org/10.1021/es502502n.

[8] Chen, W., Ouyang, Z.Y., Qian, C., Yu, H.Q., 2018. Induced structural changes of humic acid by exposure of polystyrene microplastics: A spectroscopic insight. Environ Pollut 233, 1–7. https://doi.org/10.1016/j.envpol.2017.10.027.

[9] Chiem, L.T., Huynh, L., Ralston, J., Beattie, D.A., 2006. An in situ ATR-FTIR study of polyacrylamide adsorption at the talc surface. J Colloid Interface Sci 297 (1), 54–61. https://doi.org/10.1016/j.jcis.2005.10.037.

[10] DeLeo, P.C., Summers, H., Stanton, K., Lam, M.W., 2020. Environmental risk assessment of polycarboxylate polymers used in cleaning products in the United States. Chemosphere 258. https://doi.org/10.1016/j.chemosphere.2020.127242.

[11] Duis, K., Junker, T., Coors, A., 2021. Environmental fate and effects of water-soluble synthetic organic polymers used in cosmetic products. Environ Sci Eur 33 (1). https://doi.org/10.1186/s12302-021-00466-2.

[12] Guo, F., Zhou, M., Xu, J., Fein, J.B., Yu, Q., Wang, Y., Huang, Q., Rong, X., 2021. Glyphosate adsorption onto kaolinite and kaolinite-humic acid composites: Experimental and molecular dynamics studies. Chemosphere 263, 127979. https://doi.org/10.1016/j.chemosphere.2020.127979.

[13] Hild, A., Séquaris, J.-M., Narres, H.-D., Schwuger, M., 1997. Adsorption of polyvinylpyrrolidone on kaolinite. Colloids Surf A: Physicochem Eng Asp 123-124, 515–522. https://doi.org/10.1016/S0927-7757(96)03795-8.

[14] Huangfu, X., Xu, Y., Liu, C., He, Q., Ma, J., Ma, C., Huang, R., 2019. A review on the interactions between engineered nanoparticles with extracellular and intracellular polymeric substances from wastewater treatment aggregates. Chemosphere 219, 766–783. https://doi.org/10.1016/j.chemosphere.2018.12.044.

[15] Huppertsberg, S., Zahn, D., Pauelsen, F., Reemtsma, T., Knepper, T.P., 2020. Making waves: Water-soluble polymers in the aquatic environment: An overlooked class of synthetic polymers? Water Res 181, 115931. https://doi.org/10.1016/j.watres.2020.115931.

[16] Jonkers, C., De Voogt, P., 2003, Nonionic surfactants in marine and estuarine environments. Vol. XL.

[17] Joseph, J., Jemmis, E.D., 2007. Red-, blue-, or no-shift in hydrogen bonds: a unified explanation. J Am Chem Soc 129 (15), 4620–4632.

[18] Kilduff, J.E., Karanfil, T., Chin, Y.P., Weber, W.J., 1996. Adsorption of natural organic polyelectrolytes by activated carbon: A size-exclusion chromatography study. Environ Sci Technol 30 (4), 1336–1343 https://doi.org/DOI 10.1021/es950547r.

[19] Laird, D.A., 1997. Bonding between polyacrylamide and clay mineral surfaces. Soil Sci 162 (11), 826–832.

[20] Lee, Y.K., Hur, J., 2020. Adsorption of microplastic-derived organic matter onto minerals. Water Res 187, 116426. https://doi.org/10.1016/j.watres.2020.116426.

[21] Li, Y., Dong, Q., Chen, J., Li, L., 2020. Effects of coaxial electrospun eugenol loaded core-sheath PVP/shellac fibrous films on postharvest quality and shelf life of strawberries. Postharvest Biol Technol 159. https://doi.org/10.1016/j.postharvbio.2019.111028.

[22] Liu, X., Xu, Q., Wang, D., Wu, Y., Yang, Q., Liu, Y., Wang, Q., Li, X., Li, H., Zeng, G., Yang, G., 2019. Unveiling the mechanisms of how cationic polyacrylamide affects short-chain fatty acids accumulation during long-term anaerobic fermentation of waste activated sludge. Water Res 155, 142–151. https://doi.org/10.1016/j.watres.2019.02.036.

[23] Margenau, H., 1939. Van der waals forces. Rev Mod Phys 11 (1), 1–35. https://doi.org/10.1103/RevModPhys.11.1.

[24] Mortland, M., Raman, K., 1968. Surface acidity of smectites in relation to hydration, exchangeable cation, and structure. Clays Clay Miner 16, 393–398.

[25] Mu, S., Guo, J., Yu, Y., An, Q., Zhang, S., Wang, D., Chen, S., Huang, X., Li, S., 2016. Synthesis and thermal properties of cross-linked poly(acrylonitrile-co-itaconate)/polyethylene glycol as novel form-stable change material. Energy Convers Manag 110, 176–183. https://doi.org/10.1016/j.enconman.2015.12.004.

[26] Narita, T., Ohtakeyama, R., Matsukata, M., Gong, J., Osada, Y., 2001. Kinetic study of cell disruption by ionic polymers with varied charge density. Colloid Polym Sci 279, 178–183.

[27] Noda, I., 2018. Two-dimensional correlation and codistribution spectroscopy (2DCOS and 2DCDS) analyses of time-dependent ATR IR spectra of d-glucose anomers undergoing mutarotation process in water. Spectrochim Acta Part A: Mol Biomol Spectrosc 197, 4–9.

[28] Noda, I., Ozaki, Y., 2005. Two-dimensional Correlation Spectroscopy: Applications in Vibrational and Optical Spectroscopy. John Wiley & Sons,.

[29] Pellegrin, B., Prulho, R., Rivaton, A., Thérias, S., Gardette, J.-L., Gaudichet-Maurin, E., Causserand, C., 2013. Multi-scale analysis of hypochlorite induced PES/PVP ultrafiltration membranes degradation. J Membr Sci 447, 287–296. https://doi.org/10.1016/j.memsci.2013.07.026.

[30] Piai, L., Dykstra, J.E., Adishakti, M.G., Blokland, M., Langenhoff, A.A.M., van der Wal, A., 2019. Diffusion of hydrophilic organic micropollutants in granular activated carbon with different pore sizes. Water Res 162, 518–527. https://doi.org/10.1016/j.watres.2019.06.012.

[31] Podoll, R.Thomas, Irwin, Katherine C., Brendlinger, S., 1987. Sorption of water-soluble oligomers on sediments.pdf. Environ Sci Technoi.

[32] Poinsignon, C., Cases, J., Fripiat, J., 1978. Electrical polarization of water molecules adsorbed by smectites. An infrared study. J Phys Chem 82 (16), 1855–1860.

[33] Primus, J.A.C.R.J., 1986. The Effect of Anionic Polyacrylamide Molecular Conformation and Configuration on Flocculation Eff ectivenesk. EnvironmentalProgress 5 (2).

[34] Qin, C., Zhang, W., Yang, B., Chen, X., Xia, K., Gao, Y., 2018. DNA Facilitates the Sorption of Polycyclic Aromatic Hydrocarbons on Montmorillonites. Environ Sci Technol 52 (5), 2694–2703. https://doi.org/10.1021/acs.est.7b05174.

[35] Qin, X., Du, P., Chen, J., Liu, F., Wang, G., Weng, L., 2018. Effects of natural organic matter with different properties on levofloxacin adsorption to goethite: Experiments and modeling. Chem Eng J 345, 425–431. https://doi.org/10.1016/j.cej.2018.03.125.

[36] Ren, H., Liu, Y., Zhang, R., Zheng, Y., Zhao, T., Han, J., Chen, C., Duan, E., 2023. Near-infrared carbon quantum dots from PEG-based deep eutectic solvents for high-accuracy quantitative analysis of naphthenic acids in wastewater. J Environ Chem Eng 11 (3), 109988. https://doi.org/10.1016/j.jece.2023.109988.

[37] Rozman, U., Kalcikova, G., 2021. The first comprehensive study evaluating the ecotoxicity and biodegradability of water-soluble polymers used in personal care products and cosmetics. Ecotoxicol Environ Saf 228, 113016. https://doi.org/10.1016/j.ecoenv.2021.113016.

[38] Safo, I., Werheid, M., Dosche, C., Oezaslan, M., 2019. The role of polyvinylpyrrolidone (PVP) as a capping and structure-directing agent in the formation of Pt nanocubes. Nanoscale Adv 1 (8), 3095–3106.

[39] Sainju, D., Lucas, R., Le Gresley, A., 2023. Evaluation of nuclear magnetic resonance spectroscopy for characterisation and quantitation of water-soluble polymers in river water. Water Res 245, 120650. https://doi.org/10.1016/j.watres.2023.120650.

[40] Thommes, M., Kaneko, K., Neimark, A.V., Olivier, J.P., Rodriguez-Reinoso, F., Rouquerol, J., Sing, K.S.W., 2015. Physisorption of gases, with special reference to the evaluation of surface area and pore size distribution (IUPAC Technical Report). Pure Appl Chem 87 (9-10), 1051–1069. https://doi.org/10.1515/pac-2014-1117.

[41] Wang, D., Zheng, Y., Deng, Q., Liu, X., 2023. Water-soluble synthetic polymers: their environmental emission relevant usage, transport and transformation, persistence, and toxicity. Environ Sci Technol 57 (16), 6387–6402. https://doi.org/10.1021/acs.est.2c09178.

[42] Wang, J., Zhao, X., Wu, F., Tang, Z., Zhao, T., Niu, L., Fang, M., Wang, H., Wang, F., 2021. Impact of montmorillonite clay on the homo- and heteroaggregation of titanium dioxide nanoparticles (nTiO2) in synthetic and natural waters. Sci Total Environ 784. https://doi.org/10.1016/j.scitotenv.2021.147019.

[43] Wu, P., Cai, Z., Jin, H., Tang, Y., 2019. Adsorption mechanisms of five bisphenol analogues on PVC microplastics. Sci Total Environ 650, 671–678. https://doi.org/10.1016/j.scitotenv.2018.09.049.

[44] Xiong, B., Loss, R.D., Shields, D., Pawlik, T., Hochreiter, R., Zydney, A.L., Kumar, M., 2018. Polyacrylamide degradation and its implications in environmental systems. NPJ Clean Water 1 (1), 17.

[45] Xu, Y., Ou, Q., He, Q., Wu, Z., Ma, J., Huangfu, X., 2022. Contribution of extracellular polymeric substances fractions to the adsorption of silver nanoparticles by activated sludge. J Environ Chem Eng 10 (5). https://doi.org/10.1016/j.jece.2022.108316.

[46] Yariv, S., 1992. The effect of tetrahedral substitution of Si by Al on the surface acidity of the oxygen plane of clay minerals. Int Rev Phys Chem 11 (2), 345–375.

[47] Yu, X., Guo, L., Liu, M., Cao, X., Shang, S., Liu, Z., Huang, D., Cao, Y., Cui, F., Tian, L., 2018. Callicarpa nudiflora loaded on chitosan-collagen/organomontmorillonite composite membrane for antibacterial activity of wound dressing. Int J Biol Macromol 120 (Pt B), 2279–2284. https://doi.org/10.1016/j.ijbiomac.2018.08.113.

[48] Żbik, M.S., Raftery, N.A., Smart, R.S.C., Frost, R.L., 2010. Kaolinite platelet orientation for XRD and AFM applications. Appl Clay Sci 50 (3), 299–304. https://doi.org/10.1016/j.clay.2010.08.010.

[49] Zhang, F., Wang, Z., Wang, S., Fang, H., Wang, D., 2019. Aquatic behavior and toxicity of polystyrene nanoplastic particles with different functional groups: Complex roles of pH, dissolved organic carbon and divalent cations. Chemosphere 228, 195–203. https://doi.org/10.1016/j.chemosphere.2019.04.115.

[50] Zhang, X., Liu, H., Huang, Z., Yin, Z., Wen, R., Min, X., Huang, Y., Liu, Y., Fang, M., Wu, X., 2016. Preparation and characterization of the properties of polyethylene glycol @ Si 3 N 4 nanowires as phase-change materials. Chem Eng J 301, 229–237. https://doi.org/10.1016/j.cej.2016.05.024.

[51] Zhang, Y., Luo, Y., Yu, X., Huang, D., Guo, X., Zhu, L., 2022. Aging significantly increases the interaction between polystyrene nanoplastic and minerals. Water Res 219, 118544. https://doi.org/10.1016/j.watres.2022.118544.

[52] Zhang, Z., Yuan, Z., Zhuang, L., Chai, J., 2021. Adsorption mechanism of polyacrylamide on kaolinite surface in the presence of Ca2+: Insights from DFT calculation. Chem Phys Lett 776. https://doi.org/10.1016/j.cplett.2021.138672.

[53] Zhao, J., Liu, F., Wang, Z., Cao, X., Xing, B., 2015. Heteroaggregation of graphene oxide with minerals in aqueous phase. Environ Sci Technol 49 (5), 2849–2857. https://doi.org/10.1021/es505605w.